Type of the Paper (Publication)

Medical video coding based on 2nd generation wavelets: Performance evaluation

M Ferroukhi[1], A Ouahabi[2*], M Attari[1], Y Habchi[3], M Beladgham[3], A Taleb-Ahmed[4]

[1] Laboratory of Instrumentation, Faculty of Electronics and Computers, University of Sciences and Technology Houari Boumediene, Algiers.
[2] Polytech Tours, Brain and Imaging INSERM U930, University of Tours, Tours, France.
[3] Electrical Engineering Department, Bechar University, Algeria.
[4] LAMIH CNRS U 8201, Valenciennes University, France. Affiliation 1; e-mail@e-mail.com
* Correspondence: ouahabi@univ-tours.fr ; Tel.: +33603894463

Abstract: The operations of digitization, transmission and storage of medical data, particularly images require increasingly effective encoding methods not only in terms of compression ratio and flow of information but also in terms of visual quality. At first, there was DCT (discrete cosine transform) then DWT (discrete wavelet transform) and their associated standards in terms of coding and image compression. After that, the 2nd generation wavelets seeks to be positioned and confronted to the image and video coding methods currently used. It is in this context that we suggested a method combining bandelets and SPIHT (set partitioning in hierarchical trees) algorithm. There are two main reasons for our approach: the first lies in the nature of the bandelet transform to take advantage by capturing the geometrical complexity of the image structure. The second reason stems in the suitability of encoding the bandelet coefficients by the SPIHT encoder. Quality measurements shows that in some cases (for low bit rates) the performances of the proposed coding compete with the well-established ones and opens up new application prospects in the field of medical imaging.

Keywords: Bandelet; medical imaging; quadtree decomposition; SPIHT coder; video coding; video quality measure.

1. Introduction and motivation

The huge amount of patient medical data recorded at every moment in hospitals, medical imaging centers and others medical organizations have become a major issue. The need for quasi-infinite storage space and efficient real-time transmission in specific applications such as medical imaging, military imaging and satellite imaging requires advanced techniques and technologies including coding methods to reduce the amount of data to be stored or transmitted. Without coding of information, it is very difficult and sometimes impossible to make a way to store or communicate big data (large volumes of high velocity and complex images, audio and video information) via the internet. The encoding of these data is obtained by eliminating the redundant or unnecessary information in the original frame which can't be identified with the naked eye.

Figure 1 recalls the key steps of video coding:

Transformation is a linear and reversible operation that allows the image to be represented in the transform domain where the useful information is well localized. This property will make it possible during the compression to achieve good discrimination, that is to say the suppression of unnecessary or redundant information. The discrete cosine transform and the wavelet transform are among the most popular transforms proposed for image and video coding.

Quantization is the step of the compression process during which a large part of the elimination of unnecessary or redundant information occurs.

Coding techniques e.g. Huffman coding and arithmetic coding [16-18] are the best-known entropy coding particularly in image and video coding.

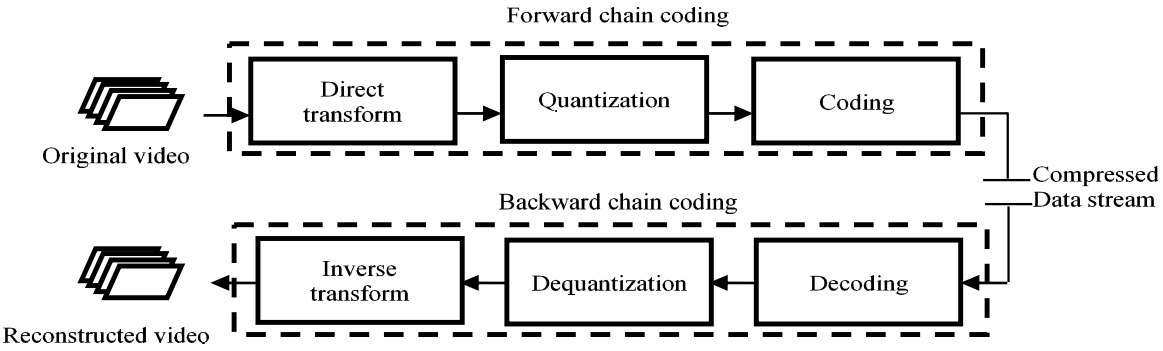

Figure 1. Simplified video coding scheme

It is well known that lossless compression methods have the advantage of providing an image without any loss of quality and the disadvantage of compressing weakly. Hence, this type of compression is not suitable for transmission or storage of big data such as video. Conversely, lossy compression produces significantly smaller file sizes often at the expense of image quality. However, lossy coding based on transforms has gained great importance when several applications have appeared. In particular, lossy coding represents an acceptable option for coding medical images. E.g., DICOM (Digital Imaging Communication in Medicine) JPEG based on DCT and DICOM JPEG 2000 based on wavelet. In this context, wavelet-based image coding, e.g. JPEG2000, using multiresolution analysis [1-2] exhibits performance that is highly superior to other methods such as those based on discrete cosine transform (DCT), e.g. JPEG.

In 1993, Shapiro introduced a lossy image compression algorithm that he called embedded zerotrees of wavelet (EZW) [3]. The success of coding wavelet approaches is largely due to the occurrence of effective subband coders. The EZW encoder is the first to provide remarkable distortion-rate performance while allowing progressive decoding of the image. The principle of zerotrees, or other partitioning structures in sets of zeros, makes it possible to take account of the residual dependence of the coefficients between them. More precisely, since the high-energy coefficients are spatially grouped, their position is effectively computed by indicating the position of the sets of low energy coefficients. After separation of the low energy coefficients and the energetic coefficients, the latter is relatively independent and can be efficiently coded using quantification and entropy coding techniques.

In 1996, Said and Pearlman proposed a hierarchical tree partitioning coding scheme called set partitioning in hierarchical tree (SPIHT) [4], based on the same basic EZW, and exhibiting better performance than the original EZW.

Video compression algorithms such as MPEG-4 and H.264 use inter-frame prediction to reduce video data between a series of images. This involves techniques such as differential coding where an image is compared with a reference image and only the pixels that have changed with respect to that reference image are coded.

MPEG allows to encode video using three coding modes:

Intra coded frames (I): frames are coded separately without reference to previous images (i.e. as JPEG coding).

Predictive coded frames (P): images are described by difference from previous images.

Bidirectionally predictive coded frames (B): the images are described by difference with the previous image and the following image.

In order to optimize MPEG coding, the image sequences are in practice coded in a series of I, B, and P images, the order of which has been determined experimentally. The typical sequence called GOP (Group of Pictures) is as follows:

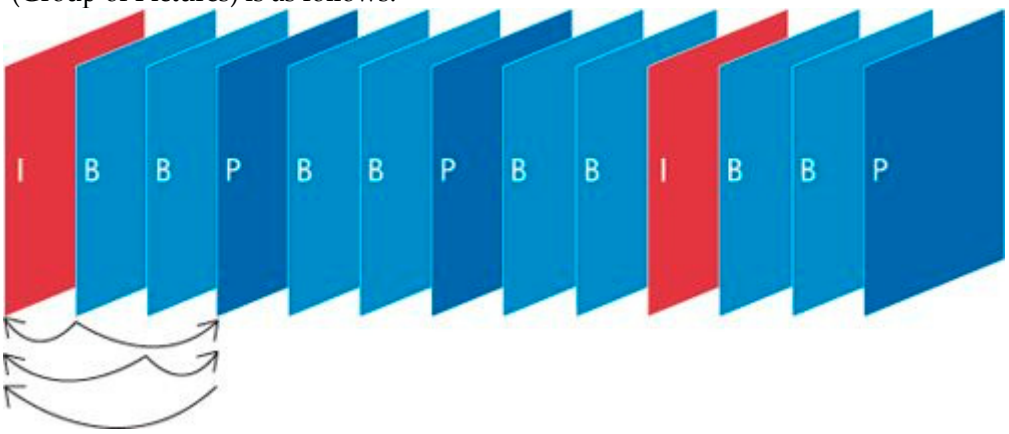

Figure 2. Typical sequence with I, B and P frames.
P frame can only refer to the previous I or P frames, while a B frame can refer to previous or subsequent I or P frames.

To evaluate the visual quality of the reconstructed video, several measurements of the quality of the MPEG video are validated in [5-6].

As a successor to the famous H.264 or MPEG-4 standards [7-8], HEVC (High Efficiency Video Coding) or H.265 standard has recently been defined as a promising standard for video coding, In June 2013 [9], the first version of HEVC was announced, and to improve the efficiency of the coding of this standard, a set of its components requires more development. In addition, this new system requires new hardware and software investments delaying its adoption in applications such as in the medical field.

This work is motivated by the prospect to offer Our motivation lies in the prospect of offering a new codec that is simple to implement with performances superior to the current H264 standard and which could compete with the H265 or HEVC standard for some applications. This superiority is based on the SPIHT algorithm and the second-generation wavelets.

One can ask: "Why using second generation wavelets (instead of classical wavelets)?"

This new generation of wavelets makes it possible to generate decorrelated coefficients, and to eliminate any redundancy by retaining only the necessary information and it is better suited to geometric data (ridges, contours, curves, or singularities). This 2nd generation wavelets consists of Xlets such as shearlets, bandelets, curvelets, contourlets, ridgelets, noiselets, contourlets, etc. These Xlets provide interesting performance in some applications, i.g. contourlets-based denoising [10], contourlets-based video coding [11-12], curvelets-based contrast enhancement [13], bandelets-based geometric image representations [14], shearlets-based image denoising [15], …

In this paper, we analyse and compare to the current state-of-the-art coding methods, the performances of a new coding method based on bandelet transform where its coefficients are encoded using the set partitioning in hierarchical trees (SPIHT).

The remainder of this paper is organized as follows: Section 2 presents and recalls the main properties of bandelet transform and Section 3 introduces bandelet-SPIHT-based video coding. Section 4 focuses on the experimental aspect and the analysis of the results. It should be noted that some preliminary results published recently in IEEE IECON 2016 [19] have been completed and analyzed in order to point out the advantages but also the limitations of the proposed method. Finally, Section 5 concludes this study.

Preprints (www.preprints.org) | NOT PEER-REVIEWED | Posted: 7 October 2018 doi:10.20944/preprints201810.0118.v1

Peer-reviewed version available at Electronics 2019, 8, 88; doi:10.3390/electronics8010088

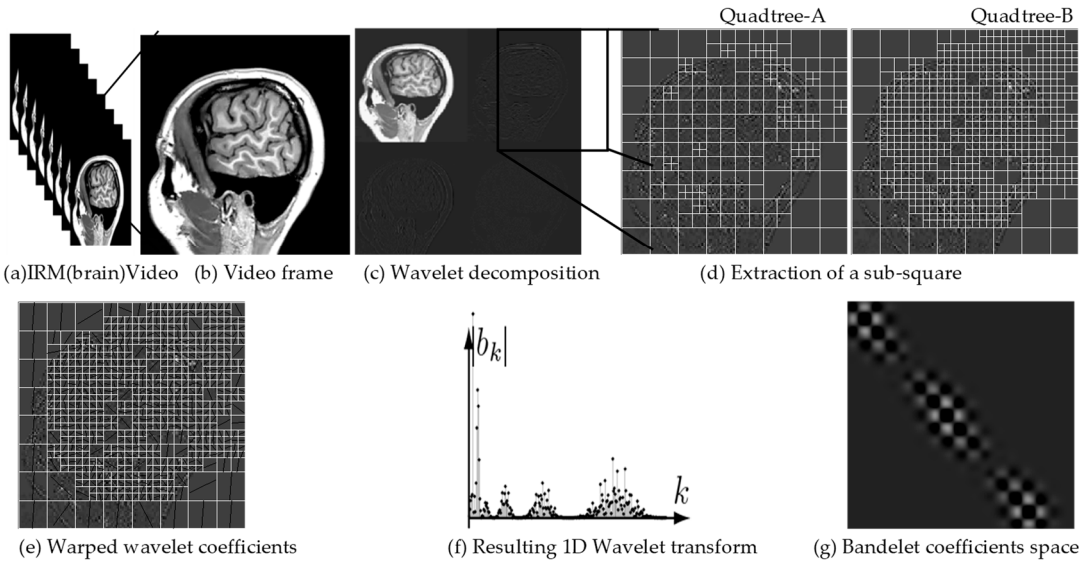

Figure 3. Example of graphical steps of the bandelet transformation algorithm

2. Bandelet transform algorithm

2.1. Bandelet transform

In order to organize intra- and inter-frames interactions, we choose the threshold to control the coding rate of the algorithm.

In step 2, 2D orthogonal or bi-orthogonal bandelet basis are performed to the original image.

The bandelization is implemented in the following steps.

Step 3:

- Performing dyadic square by recursive split of the original wavelet transform.
- Figure 3 graphically summarizes the main steps of bandelet transform illustrated on a brain MRI frame.
- Select each split dyadic square.

1D discrete wavelet transform is performed and stored in 2D image of the same size as projected result of the sampling location along potential directions and sorting 1D points result from left to right. The correct threshold and the good direction acquire a smaller approximation error.

To control the error between the recovered and the original signals for a fixed number of parameters (number of bits, quantization step and Lagrangian multiplier), a Lagrangian function is used to provide optimal direction A better bandelet is, indeed, defined by minimizing a Lagrangian cost function. Moreover, the Lagrangian minimization requests no information on regularity.

The zigzag scanning order is used in low-scale to aggregate wavelet coefficients in the upper-left corner of the output square.

2.2. Geometric flows

The bandelet bases are based on an association between the wavelet decomposition and an estimation of the image information of geometric character. The estimation of the geometry is done by studying the contours present in an image. A contour is then seen as a parametric curve that will be characterized by its tangents. To do this, we look for gradients of significant importance in the frame.

Around each region of frames, the local geometry directions, in which the frame has regular variations in the neighborhood of each pixel, are determined by two-dimensional geometric flow of a vector field, instead to describe the geometry of the frames through edges.

Preprints (www.preprints.org) | NOT PEER-REVIEWED | Posted: 7 October 2018 doi:10.20944/preprints201810.0118.v1

Peer-reviewed version available at Electronics 2019, 8, 88; doi:10.3390/electronics8010088

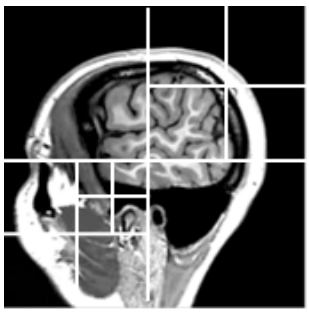

Figure 4. Example of quadtree decomposition

2.3. *Quadtree division process*

In the discussed algorithm, on each dyadic square and scale, we apply the bandelet transform; it is evidently a redundant transformation. The best segmentation represented as a quadtree is obtained by the using of the Lagrangian optimization. An example of a quadtree area division is shown in Figure 3.

In order to minimize the distortion rate, we use a parallel vertical or horizontal flux in each dyadic square. The macro block is considered regular uniformly, in the case where there is no geometric flow and the wavelet basis is used. Otherwise, deformed wavelets replaced wavelet bases, as explained in [20-21].

All directions in each block acquired by quadtree decomposition are tested, where for a given quantization step the best quadtree requires a minimization of Lagrangian.

$$L\left(f_d, R\right) = \left\| f_d - f_{dR} \right\|^2 + \lambda Q^2 \sum_j \left(R_{jS} + R_{jG} + R_{jB} \right) \quad (1)$$

where

f_d : The original signal.

f_{dR} : The recovered signal using inverse 1D wavelet transform.

R_{jS} : The bits number needed to encode the dyadic segmentation.

R_{jG} : The bits number needed to encode the geometric parameter.

R_{jB} : The bits number needed to encode the quantized bandelets coefficients.

λ: The Lagrangian multiplier is chosen to be equal to $3/28$, for a justification of this value see [22].

Q : The quantization step.

Table 1. Details and characteristics of all standards tested video

Medical sequences	Number of frames	Number of frames/ Second (Hz)	Width× Height	Video format
Brain (MRI sequence)	144	29.97	240×240	AVI
Bladder (Cancer)	662	29.97	480×320	AVI
Heart	87	29.97	340×336	AVI
Abdomen/ pelvis	295	29.97	340×352	AVI
Coronary angiography	594	29.97	360×360	AVI

Preprints (www.preprints.org) | NOT PEER-REVIEWED | Posted: 7 October 2018 doi:10.20944/preprints201810.0118.v1

Peer-reviewed version available at Electronics 2019, 8, 88; doi:10.3390/electronics8010088

The following steps implement the quadtree structure.

For each dyadic square S the value $L(S) = L(f_d, R)$ of the Lagrangian is restricted to S :

- Initialize the quadtree with the square S of size L and initialize $L_0(S)$.
- (S_1, S_2, S_3, S_4) are the fourth sub-squares defended for each square S, and $L'(S) = L_0(S_1) + L_0(S_2) + L_0(S_3) + L_0(S_4) + \lambda Q^2$ is the Lagrangian of the sub-tree
- The sub-squares should be merged if $L(S) < L'(S)$. If so, declare S as a leaf and record the optimal geometry. Update $L_0(S) = min\left(L(S), L'(S)\right)$.

Repeat the previous step for each square S of size $2L$.

2.4. *Warped wavelet along geometric flows*

In order to perform the complex geometry and remove the redundancy of orthogonal wavelet coefficients, bandelet basis decomposition is applied with a fast application of the geometric flow, quadtree decomposition, warping and bandeletization.

In each dyadic square at each scale, the geometric flow it used to warp the wavelet basis along the direction regularity. After warping, the next step is to construct bandelets by applying a bandeletization procedure.

The function of wavelet includes high-pass filters and the vanishing moments at lower resolutions, this is valid for vertical and diagonal detail coefficients, but not for horizontal detail coefficients. The problem of regularity along the geometric flow is due to the function of scaling where it includes low-pass filters and does not have the vanishing moment at lower resolutions.

To take advantage of regularity along the geometric flow for horizontal detail coefficients, the deformed wavelet basis is bandeletized by replacing the horizontal wavelet with modified horizontal wavelet function. In near of singularity, the wavelets coefficients correlations are removed by using bandeletization operation.

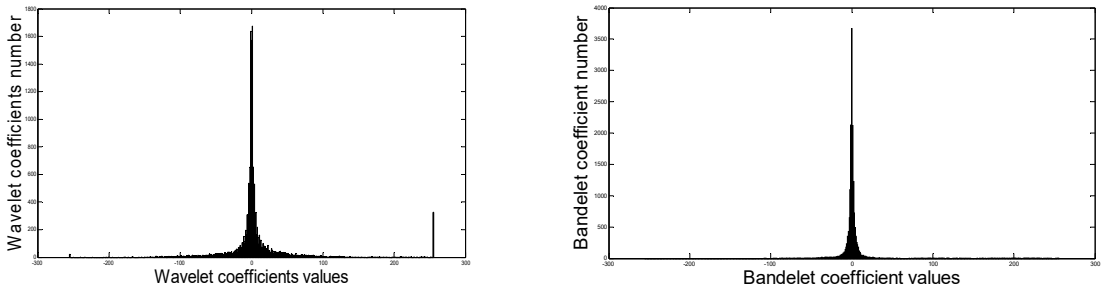

(a).Wavelet (b). Bandelet

Figure 1. Analyses histogram of bandelet and wavelet coefficient values

After warping and bandeletization operations, the regions are regular along the vertical or horizontal direction. In the end, warped wavelets are used to compute bandelet coefficients with 1D discrete wavelet transform than are encoded using SPIHT coder.

The next section is based on the principal that the most significant coefficients are achieved by the bandelet transform. In the applications of time constraints, this result confirms that our approach can be used.

Figure 4 illustrates this feature and compares wavelet and bandelet coefficients histograms results. Therefore, the SPIHT encoder, primarily applied to the wavelet results, will become Bandelet-SPIHT in this contribution.

3. Process of encoding

SPIHT algorithm [4] is one of the most efficient encoder nowadays, were it used in many applications [23-24]; whose special performances show its outperform to the JPEG 2000 in many practical situations. The list of effectiveness values symbols, are not used by SPIHT encoder such as EZW [25].

The SPIHT algorithm takes up the principles evoked in EZW while proposing to recursively partition the coefficient trees. Thus, where EZW encodes an isolated insignificant coefficient, SPIHT performs a recursive partitioning of the tree so as to determine the position of the significant coefficients in the descendant of the considered coefficient. The significant coefficients are coded similarly to EZW: their sign is sent as soon as they are identified as significant coefficients and they are added to the list of coefficients to be refined.

This algorithm also works by bit planes. The Bits sent during the significance pass correspond to the program executed at the encoder during the execution of the classification algorithm of significant and insignificant coefficients. By following the same program, the decoder remains synchronous with the decisions of the encoder and finds the same classification.

In each pass of SPIHT, the only wavelet coefficients are encoded with magnitudes exceeding a certain halved threshold values where is defined as:

$$T_p = 2^n, n = log_2 \left[\max_{(i,j)} \left| c(i,j) \right| \right] \quad (2)$$

Where:

$p = 0,1,\ldots,P$ denote the number pass

$c(i,j)$ is the coefficient at position (i,j) in frame.

The coefficients sets are ordered in spatial orientation trees, with roots in the lowest frequency subband.

The following is the three descending nodes set to correspond to wavelet coefficients at coordinates (i,j):

- Offspring set denoted by $O(i,j)$ in the same spatial orientation. Except for lowest level nodes that have four offspring.
- Type A set denoted by $D(i,j)$.
- Type B set (excluding the offspring) denoted by $L(i,j) = D(i,j) - O(i,j)$.

The resulting bandelet coefficients are ordered according to the its test of significance and stored in three separate sets of lists: list of insignificant sets (LIS), list of insignificant pixels (LIP) and list of significant pixels.

During the initialization step, added pixels to LIP are tested, added descendants sets to LIS are sequentially assessed and significant pixels are stored in initial empty list LSP.

The coding operation being with LIP, if pixels are insignificant, it stays in LIP; otherwise, pixels moved towards LSP.

Also for LIS, insignificant pixels stay in LIS. The significant pixels are divided into significant A-type set where will be divided into B-type set and four pixels; type B set is added to the end of LIS, while the remainders are examined for significance.

The principal proposed coding method is formulated as follows:

- Step1: Medical videos input
- Step2: Performing 2D discrete wavelet transform to decompose sequences into a subband.

- Step3: Decompose the frame recursively into the equal squares
- Step4: The geometric flow is applied to the each square.
- Step5: Warping the discrete wavelets along the geometric flux.
- Step6: Perform the 1D discrete wavelet transform to bandelize the wavelet bases.
- Step7: SPIHT encoded the resulting bandelets coefficients.

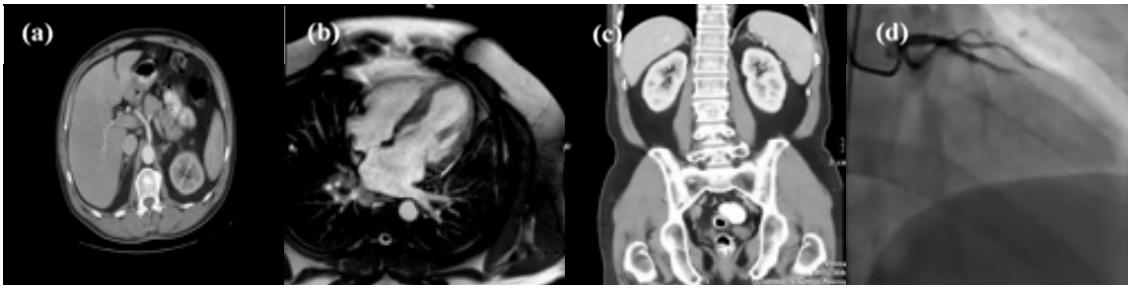

Figure 5. Medical video used for assessment
(a) Bladder cancer; (b) Heart; (c) Abdomen/Pelvis; (d) Coronary angiography.

- Step8: Gauging the quality of the recovered video sequences according to both objective and subjective criterions.

4. Experimental results

We proposed in this work, a new algorithm for medical video coding based on the bandelet transform coupled by SPIHT coder that detect complex geometric and reduce different existing redundancy in video.

The accuracy of the algorithm is tested in a bit-rate range varies from 0.1 to 0.5Mbps on some sized medical video sequences; each sequence has variable number of frames, and frame rate equal to 29.97 frames/second. The set tested medical videos are illustrated in Figure 5.

The perceived quality of recovered frames has been measured. Moreover, a comparison between Bandelet-SPIHT and the wavelet transform using SPIHT encoder, MPEG-4, and H.26x, showed promising results.

4.1. Warped wavelet along geometric flows

The characteristic of the multimedia services quality is summarized in a single term of the quality of the experience [26-27], especially, with the appearance of digital video coding, storage, and transmission systems and their fundamental limitations in the measuring the quality of video.

The National Telecommunications and Information Administration (NTIA) is one of the pioneered organizations were it general models for estimating video quality [28], it is adopted with the American National Standards Institute (ANSI) and included in The International Telecommunication Union (ITU) as a normative method [29]. Also, this domain recognized other organizations were having performed major research efforts [30-31].

The objective metrics are used to judge the performance of proposed algorithm and the higher quality of the reconstructed frames is measured [32-34].

Preprints (www.preprints.org) | NOT PEER-REVIEWED | Posted: 7 October 2018 doi:10.20944/preprints201810.0118.v1

Peer-reviewed version available at Electronics 2019, 8, 88; doi:10.3390/electronics8010088

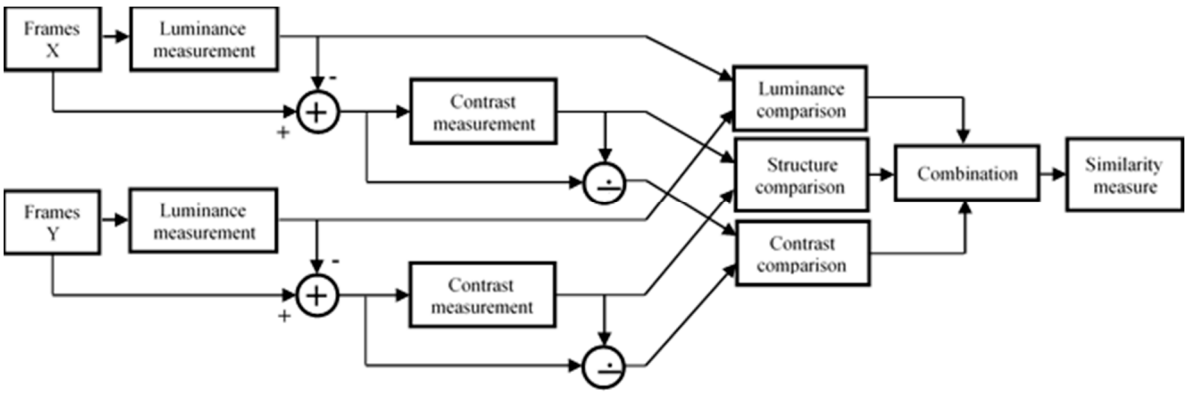

Figure 6. Block diagram of the SSIM measurement system

The peak signal-to-noise ratio (PSNR) represents an objective evaluation parameter for the measurement of image quality, is defined as follows:

$$PSNR = 10\log_{10}\left(\frac{\left(2^{n}-1\right)}{MSE}\right) \quad (2)$$

where

- $\left(2^{n}-1\right)$ is the dynamic of the signal (the maximum possible value for a pixel). In the standard case of an image where the components of a pixel are coded on $n = 8$ bits, $\left(2^{n}-1\right) = 255$.
- MSE represents the mean square error between two frames, namely the original frame and the recovered frame of size and is given by

$$MSE = \frac{1}{MN}\sum_{i=1}^{M}\sum_{j=1}^{N}\left(f\left(i,j\right)-f_{r}\left(i,j\right)\right)^{2} \quad (3)$$

The PSNR is an easy, fast and very popular quality measurement metric, widely used to compare the quality of video encoding and decoding. Although a high PSNR generally means a good quality reconstruction, but this is not always the case. Indeed, PSNR requires original image for comparison, but this may not be available in every case, also PSNR does not correlate well with subjective video quality measures, so is not very suitable for perceived visual quality [35]. Hence, the interest in considering a measure of structural similarity (SSIM) adapted to the human visual system. SSIM index introduces three key features: luminance contrast and structure This metrics is defined in (4) and the block diagram of the SSIM measurement system is represented in Fig 6:

$$l\left(x,y\right) = \frac{2M_{x}M_{y}+C_{1}}{M_{x}^{2}+M_{y}^{2}+C_{1}} \quad (5)$$

where

M_x and M_y are the mean intensity of the signal x and y defined by $M_x = \frac{1}{N}\sum_{i=1}^{N}x_i$ and $M_y = \frac{1}{N}\sum_{i=1}^{N}y_i$ respectively.

$C_i = K_i^2 D^2$, $i = 1,2$, *and* K_i is a constant, such as $K_i \ll 1$ and D is the dynamic range of the pixel values ($D = 255$ corresponds to a grey-scale digital image when the number of bits/pixel is 8).

The contrast comparison function c takes the following form:

$$c\left(x,y\right) = \frac{2\sigma_{x}\sigma_{y}+C_{2}}{\sigma_{x}^{2}+\sigma_{y}^{2}+C_{2}} \quad (6)$$

where

$$\sigma_{x} = \left(\frac{1}{N-1}\sum_{i=1}^{N}\left(x_{i}^{2}-\left(M_{x}\right)^{2}\right)\right)^{1/2}$$

The structure comparison function s is defined as follows:

Preprints (www.preprints.org) | NOT PEER-REVIEWED | Posted: 7 October 2018 doi:10.20944/preprints201810.0118.v1

Peer-reviewed version available at Electronics 2019, 8, 88; doi:10.3390/electronics8010088

$$s(x,y) = \frac{\sigma_{xy} + C_3}{\sigma_x \sigma_y + C_3} = \frac{cov(x,y) + C_3}{\sigma_x \sigma_y + C_3} \quad (7)$$

$C_3 = \frac{C_2}{2}$ and $cov(x,y) = M_{xy} - M_x M_y$

with $M_{xy} = \frac{1}{N-1}\sum_{i=1}^{N} x_i y_i$

Hence, the explicit expression of the structural similarity (SSIM) index is:

$$SSIM(x,y) = \frac{(2M_x M_y + C_1)(2\sigma_{xy} + C_2)}{(M_x^2 + M_y^2 + C_1)(\sigma_x^2 \sigma_y^2 + C_2)} \quad (8)$$

where

$$\sigma_{xy} = \left(\frac{1}{N-1}\sum_{i=1}^{N}\left((x_i y_i)^2 - (M_{xy})^2\right)\right)^{1/2}$$

Generally, over the whole video coding, a mean value of SSIM is required as Mean SSIM (MSSIM):

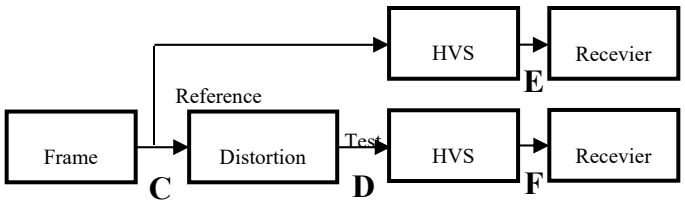

Figure 7. Diagram of the visual information fidelity (VIF) metric.

$$MSSIM(f, f_r) = \frac{1}{L}\sum_{i=1}^{L} SSIM(f_i, f_{ri}) \quad (9)$$

where and are the contents of frames (original and recovered respectively) at the ith local window (or sub-image), and is the total of local windows number in frame.

The MSSIM values exhibit greater consistency with the visual quality.

In 2006, Sheikh and Bovik [36] proposed a new paradigm for video quality assessment: information video fidelity (VIF). This criterion quantifies the Shannon information that is shared between the original and recovered images relatively to the contained information in the original image itself. It uses natural scene statistics modelling in conjunction with an image-degradation model and a human visual system (HVS) model.

Visual Information Fidelity uses the Gaussian scale mixture model (GSM) in the wavelet domain. To obtain VIF one performs a scale-space-orientation wavelet decomposition using the steerable pyramid and models each subband in the source as $C = SU$, where is a random field of scalars and is a Gaussian vector.

The distortion model is where is a scalar gain field and is an additive Gaussian noise.

VIF then assumes that the distorted and source images pass through the human visual system and the HVS uncertainty is modelled as visual noise and for the source and distorted image respectively.

The model is then:

Reference signal $E = C + N$ (10)

Test signal $F = D + N$ (11)

Where E and F denote the visual signal at the output of the HVS model from the reference and the test videos respectively, from which the brain extracts cognitive information.

The VIF measure takes values between 0 and 1, where 1 means perfect quality and is given by:

Preprints (www.preprints.org) | NOT PEER-REVIEWED | Posted: 7 October 2018 doi:10.20944/preprints201810.0118.v1

Peer-reviewed version available at Electronics 2019, 8, 88; doi:10.3390/electronics8010088

$$VIF = \frac{\sum_j I\left(C^j; F^j / s^j\right)}{\sum_j I\left(C^j; E^j / s^j\right)} \qquad (12)$$

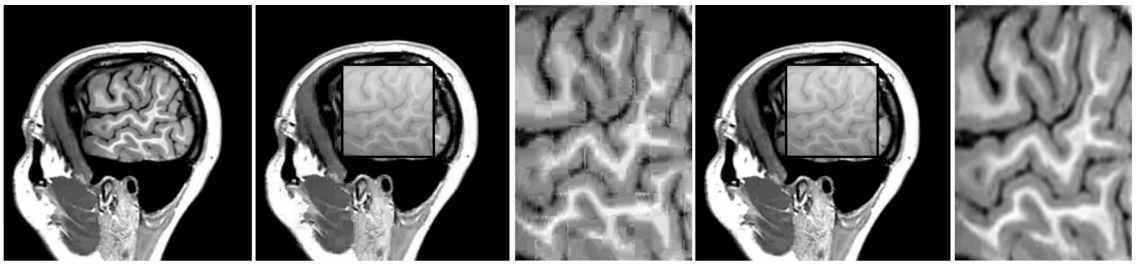

a. Original b. GALL5/3 filter c. CDF9/7 filter

Figure8.Recovered frames using:

(b). Bandelet(GALL5/3)-SPIHT and (c). Bandelet(CDF9/7)-SPIHT at 0.2Mbps.

where, $I(X;Y/z)$ is the conditional mutual information between X and Y, given z; C denotes the random field from a channel in the original image, s^j is a realization of S^j for a particular image and the index j runs through all the sub bands in the decomposed image.

4.2. Choice of the perfect filter and transform

In this part, MRI video is encoded with performing of the Bandelet-SPIHT algorithm for various bit rates. Pixels resolution MRI images is made using different filters, where each with its own peculiar properties (filter orders, symmetry and compact support) has been investigated. In order to find the best objective measures filter for video compression, the pioneer biorthogonal families was considered, thus the wavelets CDF9/7 (Cohen-Daubechies-Feauveau) and GALL5/3 (GENERATING ANY LEVELS LE) are used, they part of the family of symmetric biorthogonal wavelets CDF.

The choices of these filters are for their simplicity, symmetry and for the support width. CDF9/7 and GALL5/3 are characterized with (9/7, 2) and (5/3, 4), respectively.

where (I/J, K), I/J and K showing the number of coefficients in decomposition low-pass filter (analysis)/ reconstitution high pass filter (synthesis) and number of vanishing moments [37-40].

After an accurate visual inspection of the images in Figure 8, we adopt the bi-orthonormal wavelets CDF9/7 rather GALL5/3 to reduce the artifacts levels. The results obtained show that the visual quality of the recovered frame using the Bandelet algorithm (CDF9/7) + SPIHT is close to the original frame.

On the other hand, we notice a presence of fuzzy areas in the case of the use of GALL5/3 filter, which is arduous to detect by a simple observation.

Comparative results between (Bandelet+SPIHT) algorithm and (Wavelet +SPIHT) applied to coronary angiography test frame at various bit rates are illustrated in Figure9.

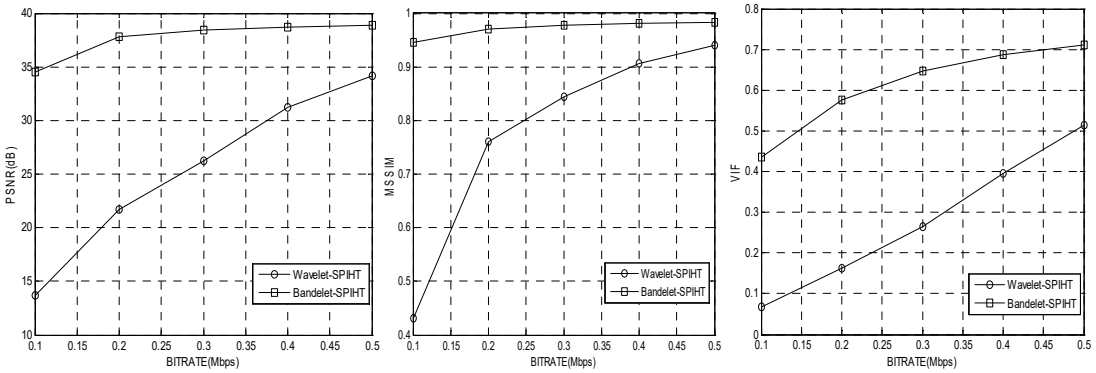

Figure9. Performance evaluation of Bandelet-SPIHT versus (Wavelet) SPIHT in terms of objective parameters.

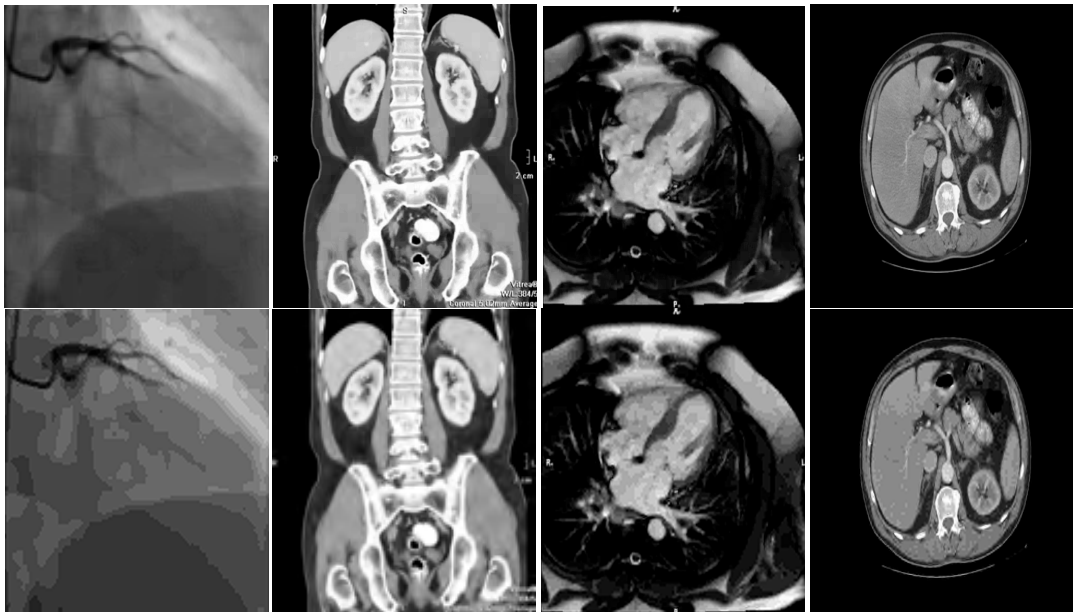

(a) (b) (c) (d)

Figure 10. Comparative quality assessments medical video using Bandelet(CDF9/7)-SPIHT (Top row), and Wavelet(CDF9/7)-SPIHT (Bottom row) at 0.5 Mbps

Figure10, shows the visual results for tested medical video. From this figures, it is clearer that the performance of (Bandelet+SPIHT), indicates that our algorithm gives best results compared to the conventional and state-of-the art coding methods and it is an apt tool to detect all special complex geometric.

While the discrete wavelet transform (SPIHT algorithm) is subject to blocking artifacts

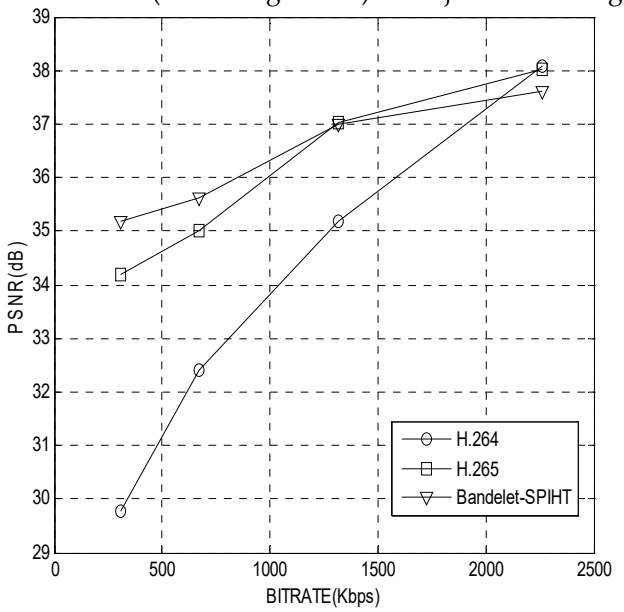

Figure 11. Comparison PSNR(dB) between the existing coding standards and proposed coding method

4.3. Bandelet-SPIHT versus standards encoder comparison

To check and prove the efficiency of the algorithm, more comparison with H.26x and MPEG standards are required. The H.264 and H.265 are known standards especially in the security industry. It is interesting to examine the maximum PSNR (dB) at the output of the proposed algorithm. As illustrated in Figure 11, the proposed method demonstrates its relatively better performance compared to the standard video coding H.264 and H.265 in terms of PSNR. For example, under 2Mbps it is clearly seen that the PSNR curves of the proposed algorithm is significantly outperformed

to the conventional standards encoders. Furthermore, for low bit rates (e.g. 1Mbps) our method can exceed H.264 and H.265 encoders by 2.41 dB and 0.23 dB respectively. Moreover, the PSNR improvements are more significant in high values.

5. Conclusion

The objective motivating our study was to propose a coding method with high performances in terms of visual quality and PSNR at low bit rates. Bandelets using SPIHT encoder is an effective condidate meeting the specific requirements of our application in the medical field and particulary in medical imaging where the quality of the image at low bit rates is a major requirement for the practitioner.

In order to show the efficiency of Bandelet-SPIHT algorithm, a set of medical sequences as test examples is considered. At low bit rates, Bandelet-SPIHT algorithm gives significantly better results (PSNR and visual quality) comparing to some cutting-edge coding techniques such as H.26x family (namely H.264 and H.265).

From this point of view, the expected goal is achieved and the prospects for application in medical imaging are promising.

Geometric image compression methods are a very dynamic search direction. One could mention the construction of transformations that adapt automatically to the geometry without the need to specify it or discrete geometry approaches ... They all agree, however, that geometry is the key to significantly improve current compression methods.

Author Contributions: Methodology, Abdeldjalil OuahabiI; Project administration, Abdelmalik Taleb-Amed; Software, Merzak Ferroukhi and Yacine Habchi; Supervision, Mokhtar Attari; Validation, Mohamed Beladgham.

References

[1] A.Ouahabi, Signal and Image Multiresolution Analysis, Wiley-ISTE: Hoboken, NJ, USA, 2012.

[2] S.Mallat, A Wavelet Tour of Signal Processing: A Sparse Way, Academic Press, third ed., USA, 2009.

[3] J.M.Shapiro, Embedded image coding using zerotrees of wavelet coefficients, IEEE Transactions on Signal Processing. 41 (1993) 3445-3462.

[4] A.Said, W.Pearlman, A new fast and efficient image codec based on set partitioning in hierarchical trees, IEEE Transactions on Circuits and Systems for Video Technology. 6 (1996) 243-250.

[5] G.W.Cermak, S.Wolf, E.P.Tweedy, M.H.Pinson, A.A.Webster, Validating objective measures of MPEG video quality, SMPTE Journal. 107 (2015) 226-235.

[6] Y.Q. Shi, S.Huifang, Image and Video Compression for Multimedia Engineering: Fundamentals, Algorithms, and Standards, second ed., CRC Press, 2000.

[7] G.J.Sullivan, J.R.Ohm, W.Han, T.Wiegand, Overview of the high efficiency video coding (HEVC) standard, IEEE Trans on Circuits and Systems for Video Technology. 22 (2012) 1649-1668.

[8] J.R.Ohm, G.J.Sullivan, H.Schwarz, T.K.Tan, T.Wiegand, Comparison of the coding efficiency of video coding standards-including high efficiency video coding (HEVC), IEEE Trans on Circuits and Systems for Video Technology. 22 (2012) 1669-1684.

[9] ITU-T Recommendation H.265, High Efficiency Video Coding, 2013.

[10] S.Sidahmed, Z.Messali, A.Ouahabi, S.Trépout, C.Messaoudi, S.Marco, Nonparametric denoising methods based on contourlet transform with sharp frequency localization: Application to electron microscopy images with low exposure time, Entropy Journal. 17 (2015) 2781-2799.

[11] S.Katsigiannis, G.Papaioannou, D.Maroulis, A contourlet transform based algorithm for real-time video encoding, SPIE Photonics Europe, Real-Time Image and Video processing Conference, Brussels, Belgium. 8437 (2012).

[12] Z.Shu, Y.Luo, G.Liu, Z.Xie, Arbitrarily shape object-based video coding technology by wavelet-based contourlet transform, IEEE International Conference on Information and Automation, Aug 2015.

[13] J.L.Starck, F.Murtagh, E.J.Candès, D.L.Donoho, Gray and color image contrast enhancement by the curvelet transform, IEEE Transactions on Image Processing. 12 (2003) 706-717.

[14] E.Le Pennec, S.Mallat, Sparse geometric image representations with bandelets, IEEE Transactions on Image Processing. 14 (2005) 423-438.

[15] G.Xie, X.Qu, J.Yan, Bandelet image coding based on SPIHT, 2nd International Symposium on Information Technologies and Applications in Education (ISITAE). (2008) 297-301.

[16] P.G.Howard, J.S.Vitter, Parallel lossless image compression using Huffman and arithmetic coding, Proceedings of the IEEE Data Compression Conference, Snowbird,March 1992.

[17] P.N.Tudor, MPEG-2 video compression, Electronics & Communication EngineeringJournal. 7 (1995) 257-264.

[18] R.Mateosian, Introduction to data compression, IEEE Micro, 16 (1996) 78.

[19] Y.Habchi, A.Ouahabi, M.Beladgham, A.Taleb-Ahmed, Towards a new standard in medical video compression, The 42nd Annual Conference of the IEEE Industrial Electronics Society (IECON2016), October 2016.

[20] G.Peyre, S.Mallat, Surface compression with geometric bandelets, ACM Transactions on Graphics. 24 (2005) 601-608.

[21] G.Peyre, S.Mallat, Discrete bandelets with geometric orthogonal filters, IEEE International Conference on Image Processing (ICIP). 1 (2005) 65-86.

[22] E. Le Pennec,S. Mallat, Sparse geometrical image approximation with bandelets, IEEE Transaction on Image Processing, 2004.

[23] S.K.Mukhopadhyay, S.Mitra, M.Mitra, An ECG signal compression technique using ASCII character encoding, Measurement Journal. 45 (2012) 1651-1660.

[24] S.Chang, L.Carin, A modified SPIHT algorithm for image coding with a joint MSE and classification distortion measure, IEEE Transactions on Image Processing. 15 (2006) 713-725.

[25] B.Rani, R.K.Bansal, S.Bansal, Comparative analysis of wavelet filters using objective quality measures, IEEE International Advance Computing Conference. (2009) 402-407.

[26] S.Winkler, P.Mohandas, The evolution of video quality measurement: from psnr to hybrid metrics, IEEE Ransactions on Broadcasting. 54 (2008) 660-668.

[27] S.Winkler, Digital Video Quality Vision Models and Metrics, John Wiley & Sons, first ed, 2005.

[28] S.Wolf, Features for automated quality assessment of digitally transmitted video, NTIA Report 264, June 1990.

[29] H.P.Margaret, S.Wolf, A new standardized method for objectively measuring video quality, IEEE Transactions on Broadcasting. 50 (2004) 312-322.

[30] D.Hands, A basic multimedia quality model, IEEE Transactions on Multimedia. 6 (2004) 806-816.

[31] A.Watson, J.Hu, J.Mcgowan, DVQ: A digital video quality metric based on human vision, Journal of Electronic Imaging. 10 (2001) 20-29.

[32] Z.Wang, A.C.Bovik, H.R.Sheikh, E.P.Simoncelli, Image quality assessment: from error visibility to structural similarity, IEEE Transactions on Image Processing. 13 (2004) 600-612.

[33] H.R.Sheikh, A.C.Bovik, Image information and visual quality, IEEE Transactions on Image Processing. 15 (2006) 430-444.

[34] M.Mark, S.Grgic, M.Grgic, Picture quality measures in image compression systems, IEEE Region 8 EUROCON. COMPUTER AS A TOOL. 2 (2003) 233-237.

[35] N.Yamsang, S.Udomhunsakul, Image quality scale (IQS) for compressed images quality measurement, Proceedings of the International MultiConference of Engineers and Computer Scientists IMECS. 9 (2009) 789-794.

[36] M.Trupti, S.D.Ruikar, Selection of wavelet for satellite image compression using picture quality measures, International Conference on Communication and Signal Processing. (2013) 1003-1006.

[37] F.Adamo, G.Andria, F.Attivissimo, A.M.L.Lanzolla, M.Spadavecchia, A comparative study on mother wavelet selection in ultrasound image denoising, Measurement Journal. 46 (2013) 2447-2456.

[38] G.Andria, F.Attivissimo, G.Cavone, N.Giaquinto, A.M.L.Lanzolla, Linear filtering of 2-D wavelet coefficients for denoising ultrasound medical images, Measurement Journal. 45 (2012) 1792–1800.

[39] L.Angrisani, P.Daponte, Thin thickness measurements by means of a wavelet transform-based Method, Measurement Journal. 20 (1997) 227-242.

[40] E.Dumic, S.Grgic, M.Grgic, New image-quality measure based on wavelets, Journal of Electronic Imaging. 19 (2010) 011018.